Lab on a Chip

View Online
Dynamic Article Links

Cite this: *Lab Chip*, 2011, **11**, 1612

www.rsc.org/loc

PAPER

A software-programmable microfluidic device for automated biology†

Luis M. Fidalgo and Sebastian J. Maerkl*

Received 28th October 2010, Accepted 15th February 2011
DOI: 10.1039/c0lc00537a

Specific-purpose microfluidic devices have had considerable impact on the biological and chemical sciences, yet their use has largely remained limited to specialized laboratories. Here we present a general-purpose software-programmable microfluidic device which is capable of performing a multitude of low- and high-level functions without requiring any hardware modifications. To demonstrate the applicability and modularity of the device we implemented a variety of applications such as a microfluidic display, fluid metering and active mixing, surface immunoassays, and cell culture. We believe that analogously to personal computers, programmable, general-purpose devices will increase the accessibility and advance the pervasiveness of microfluidic technology.

Microfluidic technology has progressed considerably in the last decade, through the development of simple fabrication methods such as soft lithography,[1] the implementation of micromechanical valves,[2,3] and the development of monolithic integration techniques.[4] It is now possible to robustly fabricate microfluidic devices containing thousands of components, enabling the implementation of complex high-throughput assays.[5,6] These fluid handling capabilities combined with its considerable economies of scale have made microfluidic technology essential in many areas including cell culture,[7–12] protein biochemistry,[5,13,14] protein crystallization[15,16] and chemistry.[17]

The developments in microfluidic integration have frequently been compared to the evolution of computer hardware.[18] Before the advent of the integrated circuit, the first electronic computers, such as the ENIAC,[19] needed to be physically re-wired before each new computing task. Analogously, 60 years later, in order to apply a microfluidic device to a new task, a new channel layout needs to be designed and physically implemented. This is a long and expensive process that requires expert knowledge of microfabrication and fluid physics.[20] The development of programmable, general-purpose computing machines transformed computers into ubiquitous information-processing tools.[21] It follows that the development of a fully software-programmable microfluidic device (PMD) could prove equally crucial for microfluidic technology. PMDs would allow the establishment of generic hardware elements whose function could be configured through an additional layer of software abstraction. With a generic architecture users could focus on adapting, developing, and disseminating software tools for their applications. Furthermore, implementing numerous applications in a generic architecture would greatly decrease development costs.

Programability and versatility have been successfully achieved in electrowetting-on-dielectric microfluidic devices.[22,23] However, integration and miniaturization in these devices is still limited as systems commonly contain only tens of active components and the unit volumes handled often fall in the microlitre range. Nevertheless, electrowetting-on-dielectric microfluidic devices have recently been applied to biologically relevant problems such as cell culturing.[24] Progress towards programmability has also been made with valve-based systems,[25,26] although current implementations tend to be limited either in their versatility, size, or integration. Jensen *et al.* presented a device featuring 64 individually addressable micromechanical valves, but the size and volume of each element is relatively large with a diameter of 1.64 mm and a volume of 120 nl.[25] Furthermore, each of the 64 micromechanical valves has to be controlled separately by one of 64 off-chip solenoid valves. The device designed by Chang *et al.*, on the other hand, features elements with considerably smaller volumes of 400 pl and a size of only a few hundred microns.[26] Furthermore, electrostatic actuation of their functional elements completely eliminates the need for off-chip control elements. Unfortunately, Chang's device only featured 7 of these electrostatically-driven control elements, severely limiting its versatility. Finally, both these examples combine the chamber units and control valves into a single functional element, which reduces the malleability of the network and the total number of functional configurations.

In this work, we present a broadly applicable, fully software-programmable microfluidic device based on microfluidic large-scale integration (MLSI).[4] Our device features 64 × 300 pl nodes controlled by 114 individually addressable valves. Each of these nodes is surrounded by up to four valves allowing variable interconnections and the implementation of arbitrary channel structures. We integrated a microfluidic multiplexer to control

School of Engineering, Institute of Bioengineering, École Polytechnique Fédérale de Lausanne, 1015, Switzerland. E-mail: sebastian.maerkl@epfl.ch; Fax: +41 2169 37830; Tel: +41 2169 37835

† Electronic supplementary information (ESI) available: Fabrication and experimental details; video sequences. See DOI: 10.1039/c0lc00537a

the array of valves, which significantly reduced the number of necessary off-chip control elements to 15. Including the fluid input control, the device contains a total of 918 micromechanical valves controlled by 21 external solenoid valves. To demonstrate the potential of this architecture we implemented various programs to perform tasks that previously required specialized devices, such as a microfluidic display,[4] active mixing and micro-formulation,[15] patterned surface immunoassays[27] and cell culture.[7]

1. Experimental

1.1. Microfluidic fabrication

Devices were molded in poly(dimethyl siloxane) (PDMS) (RTV 615, General Electric) following a fabrication protocol adapted from that described previously by Hansen *et al.*[15] In order to individually route each core valve while maintaining adequate channel and valve dimensions, we placed the routing channels and the valves on two separate layers interconnected through microfluidic vias.[28,29] Vias were formed by spin coating a PDMS film thinner than the combined height of the SU8 features from which valves and vias were molded. This resulted in a perforated membrane to which the routing layer was aligned. After bonding, this combined stack was aligned to the PDMS layer containing the flow and multiplexer channels. We found this method to be robust and efficient as no additional handling steps are required. A full description of the layer stack and fabrication details can be found in the ESI.†

1.2. Device operation

Pneumatic valves were operated by solenoid valves (Pneumadyne Inc.) connected to a PC computer through a custom-made control box. Typical operation pressures were 5, 25 and 55 psi for the flow, control and multiplexer layers, respectively. The software used to address the solenoid elements was written in Visual Basic. The programs were based on a series of pneumatic operations aimed at addressing each core valve (Fig. 2a–e). Complex protocols were created by scripting sequential actuation of core valves giving rise to specific geometries on the PMD to shunt fluid according to the assay requirements.

1.3. Surface immunoassays

Antibody patterns were created on the glass surface of the device by sequentially flowing a blocking solution of 2% bovine serum albumin (Sigma) in water and antibody solutions through selected nodes. The proteins rapidly adsorbed to the glass surface without the need of additional coupling chemistry. The antibodies used were anti-GST Alexa-647 and anti-GFP (Abcam), diluted to 1 : 100 in phosphate buffered saline buffer (PBS) before use. eGFP (BioVision) was diluted to 1 : 500 in 2% BSA dH_2O. BSA blocking, antibody deposition and eGFP deposition were performed by flowing the solution of interest for 10 min followed by a 5 min rinse with PBS. In the construction of the A-GST pattern longer deposition times were used for complex channel geometries to compensate for their higher resistance. In the eGFP immunoassay, BSA was flowed through the channels where antibody was deposited before flowing eGFP to prevent any non-specific binding. After flowing GFP, BSA was flowed through the same rows to remove any non-specifically bound protein.

1.4. Cell culture

The yeast strains used were wild type (BY4741, MATa his3Δ1 leu2Δ0 met15Δ0 ura3Δ0) and a mutant expressing mCherry under the control of the PHO5 promoter (BY4741; trp1Δ::P_{PHO5}-mCherry-Kan). Liquid cultures were prepared by inoculating samples of 3 ml synthetically defined medium (Sigma) that were incubated overnight and diluted 1 : 2 in fresh medium 4 h before use. Standard culture medium contained 10 mM inorganic phosphate, whereas induction medium contained no inorganic phosphate. On- and off-chip culturing was conducted at 30 °C.

2. Device architecture and operation

The PMD's generic architecture consists of a network of intersecting channels controlled by an array of 114 independently addressable elastomeric valves (Fig. 1). We used a 7-bit binary multiplexer and latching[4] to independently control the 114 core valves with only 15 inputs (Fig. 2a–e). When all valves are pressurized, each of the 64 network nodes becomes a 300 pl reaction vessel (Fig. 1c). Opening a sequence of valves connecting nodes between the entrance and exit creates a route through the network into which flow can be directed. The input–output tree controls which solutions are introduced at any given time (Fig. 1a). Due to complete control over the connectivity of the network nodes, there are no restrictions in the geometry of that route and complex channels can be implemented within seconds and in real-time (Fig. 2f, Video S1†).

We observed that when closing core valves fluid was occasionally displaced between nodes in an uncontrolled manner. Fluid displacement is inherent to this type of zero dead-volume valve, but in a closed network design such as ours it can induce cross-talk between nodes. We designed and implemented fluidic capacitors to accommodate the fluid displaced when closing core valves (Fig. 1c, Fig. S2†). The capacitors consisted of square spaces located above each node into which the PDMS membrane could deflect. Fig. S2† contains a schematic of a node and the corresponding capacitor when the adjacent core valves are either open or closed. It also shows micrographs of two devices with closed core valves after loading a red dye, and the elimination of the cross-talk between nodes in the device containing capacitors.

Several critical parameters determine the usability of a PMD, the speed of device reprogramming being one of the most important aspects. In our device, the minimal time required to actuate a core valve is below 100 ms. The shortest time to create a route through the network amounts to 1.6 s and can extend to several seconds, depending on the complexity of the path or the number of core valves that need to be actuated to create the path. A second critical parameter for the performance of our reconfigurable platform is its durability. PDMS elastomeric valves have been shown to withstand extended use without signs of wear.[2] Operating our devices at the speeds indicated did not lead to performance reduction after running a display routine continuously for more than 18 h or a cell culture program for

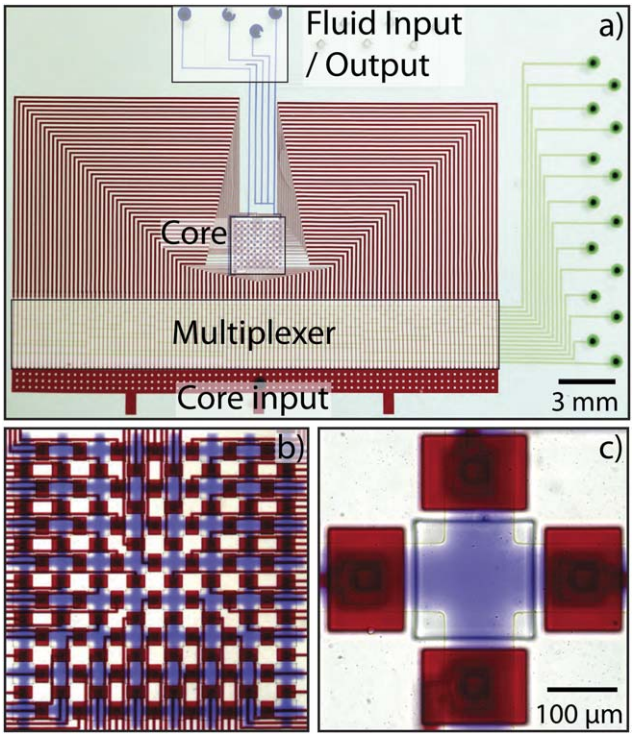

Fig. 1 Software-programmable microfluidic platform. (a) Photograph of the PMD outlining its constitutive modules. A channel network (blue) sits at the center of a core valve array (red) controlled by a 7-bit microfludic multiplexer (green) and a master core input. A separate set of valves controls the flow of liquid into the network. (b) Micrograph of the central channel network. Individually addressable valves surround each network node providing full control over their connectivity. Routing channels access valves through microfluidic vias from a separate layer above. (c) Micrograph of a network node. Each node constitutes a 300 pl vessel and consists of several core valves and a microfluidic capacitor.

24 h. In both cases the number of multiplexing and valve actuating operations exceeded 10^5. Finally, a measure of the flexibility of a reconfigurable platform is the number of unique configurations it can achieve. In our case, without taking into account the input module, these amount to 2^{114} or over 2×10^{34} states.

Our PMD represents a versatile and inexpensive microfluidic platform capable of handling volumes as small as 300 pl, with a total footprint of 20 × 30 mm and requiring 21 external controls, 15 for multiplexing and 6 to control fluid input. Its operation is simplified through a layer of abstraction making it particularly suitable for use by a broad spectrum of scientists with no microfluidic expertise. The following sections describe the set of fluidic operations used to build up more complex protocols as well as implementations of representative applications traditionally performed on specialized devices.

3. Applications

3.1. Microfluidic display

To demonstrate the capabilities of our microfluidic device for automated node addressing and compound loading, we wrote a simple program that created dye patterns resembling letters. To create each pattern, the program determined which nodes needed to be "re-written" into a new state: red or white. The program created a fluidic path from input to output to address each node. Once the path was created, the correct solution—red dye or water—was flown through the node until the contents of the node were completely replaced. Creating the fluidic path required 1.6 s for each node, whereas replacing the contents took 6 s and an approximate volume of 80 nl. Iteratively repeating this addressing and loading procedure yielded the intended pattern that was stored for a given time before continuing with the next one (Fig. 2g, Video S2†).

In addition to the wait times for valve actuation and fluid loading, the only input the user must provide is the sequence of letters to be displayed. We believe this example illustrates how easily users can determine the location of compounds within the network. Moreover, it also shows how the loading procedure can be carried out in a few minutes, using only minute amounts of the compounds of interest. Simple modification to the software program could adopt this loading routine to almost any basic microfluidic device functionality and more specialized applications such as immunoassays as described in the next section.

3.2. Surface immunoassays

Immunoassays constitute a fundamental tool in biological research, and their miniaturization has received significant attention.[27,30] To illustrate how surface immunoassays could easily be implemented in our reconfigurable platform we carried out two separate experiments based on the dynamic channel reconfiguration described above. In the first experiment, we used sequential channel routing across the network to create a surface pattern of a fluorescently labeled anti-GST (A-GST) antibody. We achieved this by selectively flowing either BSA or an

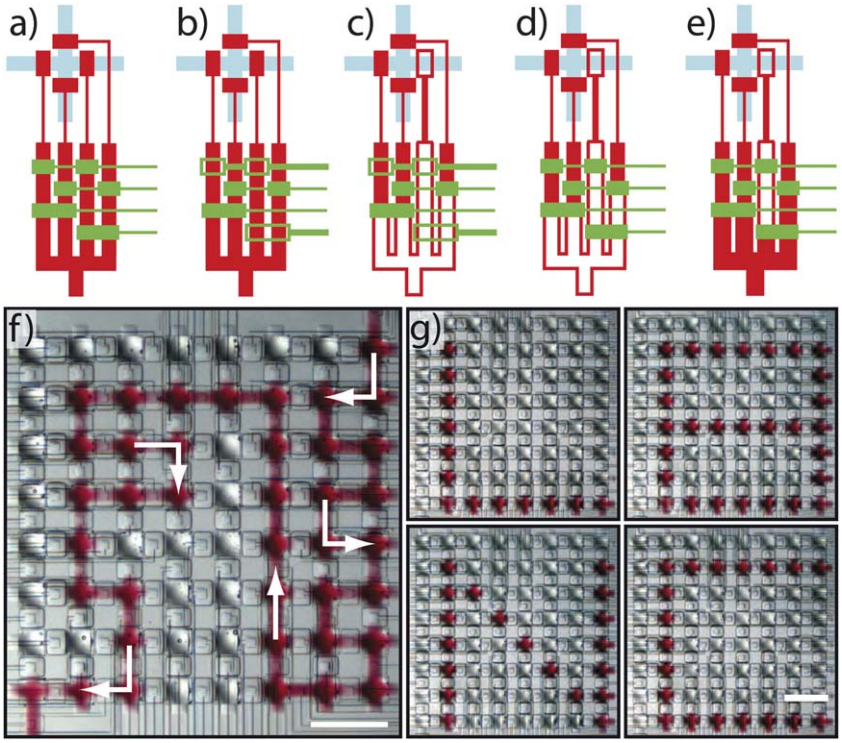

Fig. 2 (a–e) Schematic diagram of the steps required to actuate core valves. All core valves are initially closed (a). To open a valve, the multiplexer is addressed to allow flow through the corresponding control channel (b). The core input valve is depressurized allowing the selected valve to open (c). Pressurizing the multiplexer stores the open state for the addressed valve (d), and allows re-pressurizing of the core input without modifying the state of the core valves (e). (f) Controlled fluid delivery in the PMD. Opening the valves between the selected nodes creates a channel across the network into which fluid can be directed. The channel was filled with red dye for visualization (Video S1†). (g) Micrographs showing red dye patterns generated through sequential node addressing and loading displaying the letters LBNC (Video S2†). Scale bars are 500 μm.

antibody solution through complex fluidic paths. When flowed through a channel, BSA deposited on the surface blocking the posterior adsorption of the antibody and therefore generating "black" areas. Flowing the antibody solution over the areas that were not exposed to BSA created the pattern later imaged with fluorescence microscopy (Fig. 3a).

In the second experiment, we used a similar approach to pattern two antibodies, the same fluorescently-labeled anti-GST and a non-labeled anti-GFP (A-GFP) antibody. We patterned these two antibodies in adjacent columns while all other areas of the network were blocked with BSA. We then flowed eGFP horizontally in alternating rows, which bound selectively to the anti-GFP antibody (Fig. 3b–c).

3.3. Micro-formulation

Microfluidic technology offers great advantages as a platform for biochemistry and chemistry, such as throughput, accuracy, and automation.[15,17] Formulation in a microfluidic environment requires higher-level functionalities such as accurate fluid metering and efficient mixing. Our PMD is well suited for both, since nodes can be used as loading units and core valves can be used for active mixing using ring mixers.[31]

We implemented a variety of ring mixer geometries, involving 12, 10 or 4 nodes (Fig. 4). Video S3† shows an image sequence were multiple ring mixers are implemented sequentially, using them to actively mix a colored dye ($Fe(SCN)_3$). We loaded a section of a 12-node ring with a dye solution that was actively mixed with the contents of the remaining nodes (Fig. 4b). Following this mixing, three 4-node rings were created at different locations, resulting in three different final concentrations of the dye (Fig. 4c). The capacity to create ring mixers at any location within the network could be beneficial not only for accurate formulation, but also for *in situ* compound dosing in multistep reactions or cell culture. The software-interface requires as input only the type and location of the mixer within the network and the desired mixing time.

The required mixing time depends on the size of the ring and varies between 30 s (4-node ring, Fig. 5b) and 150 s (12-node ring, Fig. 5a). To measure the time required for mixing we measured pixel intensity at a fixed position in the ring during an image sequence of dye mixing. Using software implemented mixers allowed us to dynamically program the peristaltic pump in our 12-node mixer to optimize mixing speeds (Fig. 5a). Mixing time increased as the number of valves used for pumping decreased, although mixing still occurred when only two valves where used. Using one valve induced no appreciable peristaltic flow and the speed of mixing was similar to that by diffusion only. Fig. 5b shows mixing curves for a 4-node ring where four pumps were used for mixing. Both curves were obtained measuring pixel intensity at the same position, but for each of them either the top or the bottom row were loaded with dye, inducing a 90° phase shift in the mixing curve. The time required to homogenize the 4-node ring was approximately 30 s.

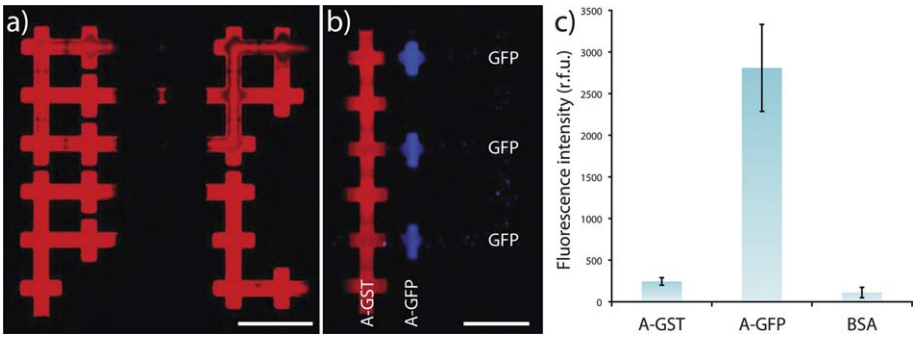

Fig. 3 (a) Fluorescence micrograph of an Alexa-647-labeled anti-GST pattern displaying the letters EPFL. Routing fluids across the network and flowing either BSA or antibody, selected regions were either protected or labeled, creating the resulting pattern. (b) Fluorescence micrograph showing a pattern of labeled anti-GST and eGFP. A-GST and A-GFP antibodies were deposited in parallel columns while the rest of the network was protected with BSA. eGFP was flowed through alternative rows from right to left. The micrograph shows A-GST deposition throughout the entire column and eGFP deposition exclusively at the intersection between the A-GFP column and the eGFP rows. Scale bars are 500 μm. (c) Quantification of the eGFP immunoassay. Measurements of the fluorescence intensity at 530 nm for the nodes at the intersection between the eGFP rows and the anti-GFP, anti-GST and BSA columns show selective eGFP deposition at selected locations. Each bar represents the average of three measurements and the error bars show one standard deviation.

Active mixing combined with fluid metering can be used to accurately formulate compositions *in situ*. Concentration gradients can easily be created by loading different quantities of a reagent in a given ring size. We created an array of dye concentrations by loading an increasing number of nodes with dye in 3 separate 4-node rings (Video S4,† Fig. 5c–d). Absorbance values extracted from the micrographs for each final concentration show good agreement with Lambert–Beer's law demonstrating the accuracy of the formulation (Fig. 5e).

In addition to using nodes as metering units, the PMD allows peristaltic pumping to accurately dose compounds.[15] We believe that the ability to generate complex mixtures confers onto the PMD a great potential for high-throughput studies in areas such as cell culture or biochemistry. One can envision integrated methods where numerous compounds could be simultaneously tested in a range of concentrations and combinations in a single experiment, significantly reducing the cost and time necessary for such studies. Furthermore, creating complex feedback dynamics with machine learning algorithms would allow a computer to dynamically adjust the concentrations or compound combinations during a screen, or even optimize the entire microfluidic layout during the screening process.

3.4. Cell culture

Cell culture is one of the most appealing applications of microfluidics. The match between the dimensions of microfluidic channels and a wide variety of cell types combined with high-throughput and compatibility with light microscopy has made miniaturized cell culture a major focus in the field. A number of specialized devices have been developed to culture bacteria,[9,12] yeast[7,10] and mammalian cells.[8,11,32] To show the potential of our PMD for cell culture we implemented a multiplexed yeast culture experiment. We loaded two yeast strains into 8 independent

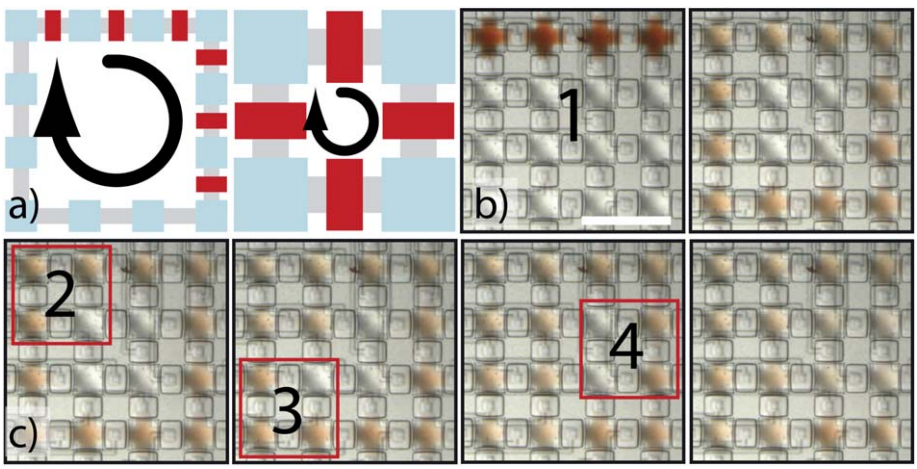

Fig. 4 Software implementation of active mixing and micro-formulation. (a) Schematic of the equivalent channels for the 12- and 4-node ring mixers. Opening a series of core valves creates a ring; actuating them repeatedly generates peristaltic flow that homogenizes its contents (Video S3†). (b) Micrographs showing a 12-node ring partially loaded with dye before and after mixing. (c) Micrographs showing 3 sequential mixing steps using 4-node rings. This combination of mixing steps results in three different dye concentrations. Scale bar is 500 μm.

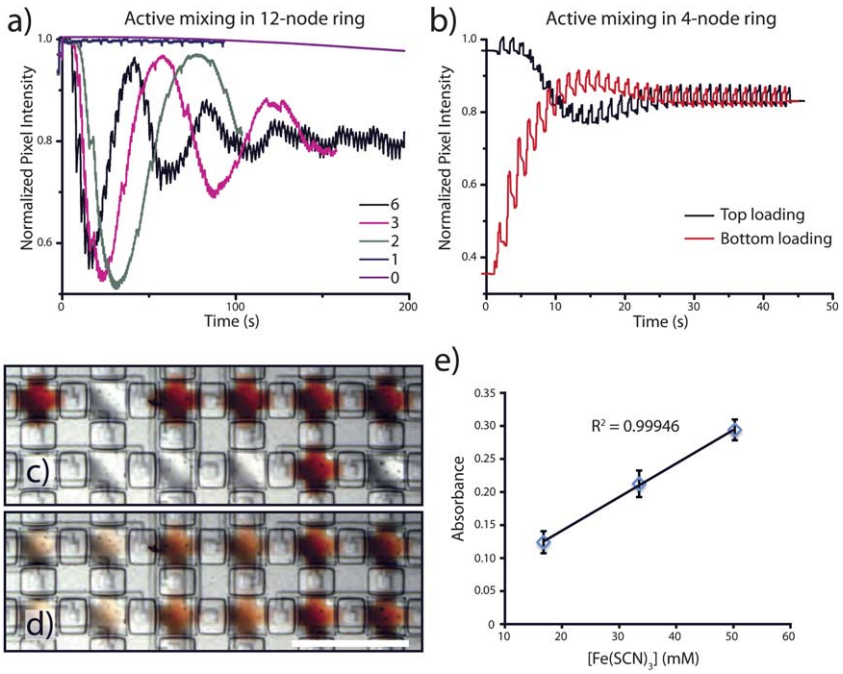

Fig. 5 (a) Active mixing in a 12-node ring using an increasing number of valves for peristaltic pumping. Mixing time increases as the number of valves decreases. The mixing time required for the fastest pump (6 valves) is approximately 150 s. (b) Active mixing in a 4-node ring using four valves for pumping. Mixing curves measured at the same point in the ring while loading either the top or bottom row show a 90° phase shift. Mixing is achieved in approximately 30 s. (c–d) On-chip parallel micro-formulation. Three different dilutions of $Fe(SCN)_3$ are prepared in separate 4-node ring mixers by loading an increasing number of nodes with an initial solution (c) before homogenizing them (d). (e) Absorbance values extracted from the micrographs for each final concentration agree with Lambert–Beer's law. Each point represents the average of four measurements and the error bars show one standard deviation.

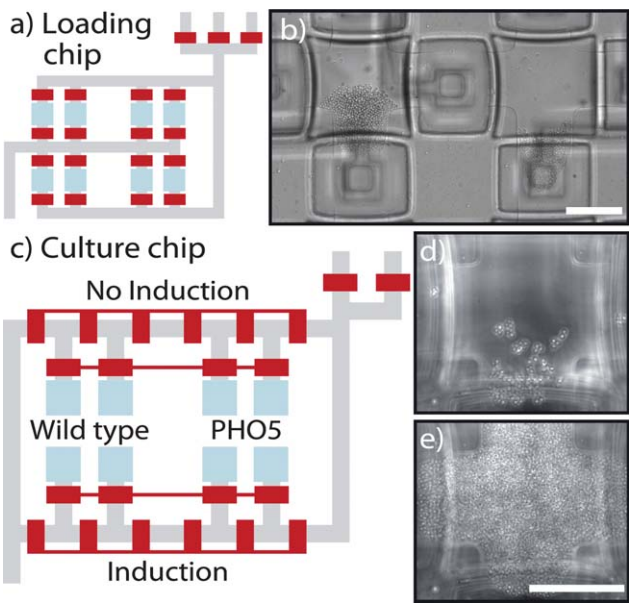

Fig. 6 Cell culture in a software-programmable device. (a) Schematic of the equivalent loading device implemented for cell trapping. (b) Micrograph of a seeded chamber (left) and a chamber being loaded (right). Flowing a yeast suspension through a partially closed valve allows cell trapping and control of seeding density (Video S5†). (c) Schematic of the equivalent cell culture device. Micrographs of (d) a chamber after seeding with wild type yeast and (e) after 12 h of culture. Scale bars are 100 μm.

growth chambers and grew them for 9 h in standard conditions. We then switched the growth condition in 4 of the 8 chambers, effectively performing 4 independent cell culture experiments in duplicate.

We conceptually implemented two microfluidic devices, one for cell loading and a second for cell culture. The loading chip allowed independent addressing of the 8 growth chambers using a path that could be partially closed using a core valve as a sieve (Fig. 6a).[33] To load cells to the desired density, a cell suspension was flowed through the sieve trapping cells in the growth chamber (Fig. 6b, Fig. S3a, Video S5†).

During culture, we needed to ensure correct compartmentalization of the cell chambers while maintaining stable media compositions over extended periods of time. To enable compartmentalized perfusion we implemented perfusion channels in addition to growth chambers (Fig. 6c, Fig. S3b–c†). The culture protocol consisted of two alternating steps: exchanging the medium in the perfusion channels while the culture chambers were closed; and allowing diffusion between culture and perfusion chambers while preventing cross-talk with adjacent culture chambers. Since there were two separate conditions on the device, these alternating steps were performed simultaneously: while one section was replenished the other was perfused and *vice versa* (Fig. S3b–c†). The period of the cycle was one minute, which ensured efficient medium replenishment as well as sufficient diffusion of nutrients between perfusion channels and culture chambers.

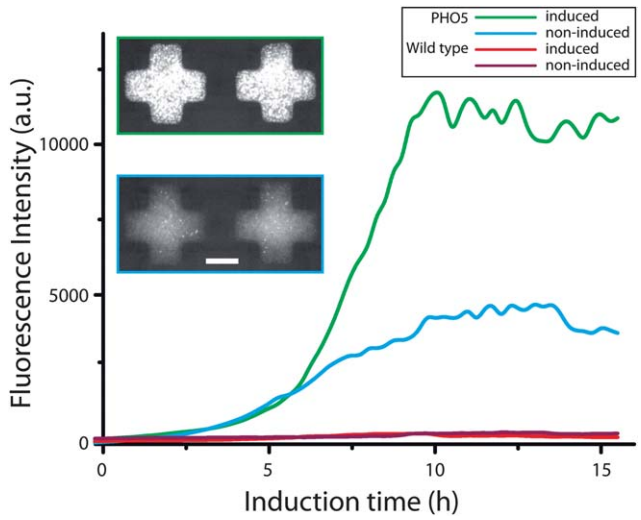

Fig. 7 Quantification of yeast induction on chip. Two strains of yeast were cultured in duplicate at two different conditions within the device. Wild type yeast remains non-fluorescent under both inducing and non-inducing conditions. A mutant expressing m-Cherry under the control of the pho5 promoter increases its fluorescence upon induction. (inset) Fluorescence micrographs of the chambers populated by the pho-5 strain under both culture conditions showing the final levels of fluorescence.

Cells were cultured in standard conditions for 9 h before induction (Fig. 6d–e, Video S6†). Following the initial growth period two chambers of each strain were induced by culturing them in the absence of inorganic phosphate while the remaining chambers continued under the original condition (Fig. 6c). We used wild type yeast as a control and a mutant strain expressing mCherry under the control of the pho5 promoter, which is induced in the absence of inorganic phosphate.[34] Fluorescence imaging shows a considerable increase in fluorescence upon induction (Fig. 7). In this experiment, we cultured each strain in duplicate under inducing and non-inducing conditions, accounting for a total of 8 simultaneous experiments. These results show the potential of PMDs for performing exceedingly complex methods such as parallel, automated cell culturing under changing conditions.

4. Conclusions

We have developed a highly-integrated PMD applicable to a wide range of tasks. We have shown that our PMD can quickly and accurately perform low- and high-level functions such as automated addressing of the network nodes to generate a display, as well as fluid metering and active mixing of compounds. Biological applications such as immunoassays and cell culturing were also successfully implemented. None of these applications required the modification of the microfluidic device hardware, but instead were fully implemented by software.

Our PMD features 64 individually addressable nodes controlled by 15 external inputs. The number of controlled valves increases exponentially with the number of inputs because of multiplexing. The limitations in increasing the number of nodes therefore stem exclusively from limitations related to the physical layout of channels and valves and their space requirements. We foresee that the current layer structure could accommodate as many as 256 nodes with only minor modifications of the routing paths. Reducing the dimensions of vias and routing channels and dividing these between multiple layers could further increase the number of nodes.

The node geometry and connectivity described here are relatively simple. Different node shapes and connectivities could be optimized for various applications while maintaining the same off-chip control hardware and software. Combining the flexibility of the PMD with a number of dedicated devices could help address specific applications while maintaining the benefits of simplicity and low cost for the end-user. Indeed, hybrid devices containing a PMD core supported by purpose built device sections may combine the advantages of both platform concepts.

Eliminating the need to physically redesign devices will drastically reduce the development time and cost of new microfluidic applications. Moreover, using PMDs will enhance dissemination of microfluidic technologies by eliminating the need for technical knowledge of microfluidic device design and fabrication, and allow researchers to quickly implement and debug their devices. Just as with computers, generating general-purpose machines and simplifying their use through software abstraction will significantly increase the pervasiveness of microfluidic devices.

Acknowledgments

We thank Arun S. Rajkumar for kindly providing both yeast strains and Nano-Tera and EPFL for funding.

References

1 Y. Xia and G. M. Whitesides, *Angew. Chem., Int. Ed.*, 1998, **37**, 550–575.
2 M. A. Unger, H.-P. Chou, T. Thorsen, A. Scherer and S. R. Quake, *Science*, 2000, **288**, 113–116.
3 W. H. Grover, R. H. C. Ivester, E. C. Jensen and R. A. Mathies, *Lab Chip*, 2006, **6**, 623–631.
4 T. Thorsen, S. J. Maerkl and S. R. Quake, *Science*, 2002, **298**, 580–584.
5 S. Maerkl and S. Quake, *Science*, 2007, **315**, 233–237.
6 S. J. Maerkl and S. R. Quake, *Proc. Natl. Acad. Sci. U. S. A.*, 2009, **106**, 18650–18655.
7 R. J. Taylor, D. Falconnet, A. Niemistö, S. A. Ramsey, S. Prinz, I. Shmulevich, T. Galitski and C. L. Hansen, *Proc. Natl. Acad. Sci. U. S. A.*, 2009, **106**, 3758–3763.
8 R. Gomez-Sjoberg, A. A. Leyrat, D. M. Pirone, C. S. Chen and S. R. Quake, *Anal. Chem.*, 2007, **79**, 8557–8563.
9 F. K. Balagadde, L. You, C. L. Hansen, F. H. Arnold and S. R. Quake, *Science*, 2005, **309**, 137–140.
10 M. R. Bennett, W. L. Pang, N. A. Ostroff, B. L. Baumgartner, S. Nayak, L. S. Tsimring and J. Hasty, *Nature*, 2008, **454**, 1119–1122.
11 P. J. Lee, P. J. Hung, V. M. Rao and L. P. Lee, *Biotechnol. Bioeng.*, 2006, **94**, 5–14.
12 T. Danino, O. Mondragon-Palomino, L. Tsimring and J. Hasty, *Nature*, 2010, **463**, 326–330.
13 D. Gerber, S. J. Maerkl and S. R. Quake, *Nat. Methods*, 2009, **6**, 71–74.
14 S. Einav, D. Gerber, P. D. Bryson, E. H. Sklan, M. Elazar, S. J. Maerkl, J. S. Glenn and S. R. Quake, *Nat. Biotechnol.*, 2008, **26**, 1019–1027.
15 C. L. Hansen, M. O. A. Sommer and S. R. Quake, *Proc. Natl. Acad. Sci. U. S. A.*, 2004, **101**, 14431–14436.
16 B. Zheng, L. S. Roach and R. F. Ismagilov, *J. Am. Chem. Soc.*, 2003, **125**, 11170–11171.
17 C.-C. Lee, G. Sui, A. Elizarov, C. J. Shu, Y.-S. Shin, A. N. Dooley, J. Huang, A. Daridon, P. Wyatt, D. Stout, H. C. Kolb,

O. N. Witte, N. Satyamurthy, J. R. Heath, M. E. Phelps, S. R. Quake and H.-R. Tseng, *Science*, 2005, **310**, 1793–1796.
18 G. M. Whitesides, *Nature*, 2006, **442**, 368–373.
19 D. Hartree, *Nature*, 1946, **158**, 500–506.
20 J. Melin and S. R. Quake, *Annu. Rev. Biophys. Biomol. Struct.*, 2007, **36**, 213–231.
21 P. E. Ceruzzi, *A History of Modern Computing*, The MIT Press, 2003.
22 M. J. Jebrail and A. R. Wheeler, *Curr. Opin. Chem. Biol.*, 2010, **14**, 574–581.
23 S.-K. Fan, T.-H. Hsieh and D.-Y. Lin, *Lab Chip*, 2009, **9**, 1236–1242.
24 I. Barbulovic-Nad, S. H. Au and A. R. Wheeler, *Lab Chip*, 2010, **10**, 1536–1542.
25 E. C. Jensen, B. P. Bhat and R. A. Mathies, *Lab Chip*, 2010, **10**, 685–691.
26 M.-P. Chang and M. M. Maharbiz, *Lab Chip*, 2009, **9**, 1274–1281.
27 E. Delamarche, A. Bernard, H. Schmid, B. Michel and H. Biebuyck, *Science*, 1997, **276**, 779–781.
28 E. Kartalov, C. Walker, C. Taylor, W. Anderson and A. Scherer, *Proc. Natl. Acad. Sci. U. S. A.*, 2006, **103**, 12280–12284.
29 J. Huft, D. J. Da Costa, D. Walker and C. L. Hansen, *Lab Chip*, 2010, **10**, 2358–2365.
30 R. Fan, O. Vermesh, A. Srivastava, B. K. H. Yen, L. Qin, H. Ahmad, G. A. Kwong, C.-C. Liu, J. Gould, L. Hood and J. R. Heath, *Nat. Biotechnol.*, 2008, **26**, 1373–1378.
31 H.-P. Chou, M. A. Unger and S. R. Quake, *Biomed. Microdevices*, 2001, **3**, 323–330.
32 C. E. Sims and N. L. Allbritton, *Lab Chip*, 2007, **7**, 423–440.
33 J. S. Marcus, W. F. Anderson and S. R. Quake, *Anal. Chem.*, 2006, **78**, 3084–3089.
34 F. H. Lam, D. J. Steger and E. K. O'Shea, *Nature*, 2008, **453**, 246–250.